Mar Biol
DOI 10.1007/s00227-006-0514-y

RESEARCH ARTICLE

Broad-band versus narrow-band irradiance for estimating latitude by archival tags

Hisham A. Qayum · A. Peter Klimley · Ronald Newton · John E. Richert

Received: 13 October 2005 / Accepted: 16 August 2006

Abstract The relative effectiveness of different bands of irradiance to estimate the latitude of archival tags was evaluated. These tags are placed on fishes in order to describe their movements during long distance migrations. Measurements were recorded of broad-band irradiance with and without a cosine collector and narrow-band irradiance of seven narrow bands with 50% attenuation 30 nm on either side of their central wavelength of 400 (violet), 450 (blue), 500 (blue–green), 550 (green), 600 (yellow), 650 (orange), and 700 nm (red). A holographic, cosine collector was used to reduce the vertical transmission of irradiance to the sensor and to increase horizontal transmission of irradiance so the sensor detected more of the diffuse irradiance penetrating the water at dawn and dusk. Daily measurements were made during seven periods of 1–2 days each, beginning 28 June (after 21 June solstice) and ending on 6 October 1999 (after September 23 equinox) of submarine irradiance at 15-s intervals at a fixed depth (10 m) and location (38.31°N; 123.08°W) in Horseshoe Cove, California. Irradiance transmission at this site is intermediate between the clearest offshore waters, where blue irradiance (450 nm) penetrates farther with depth than green irradiance (550 nm) and most oceanic and coastal waters, where green penetrates farther than blue irradiance. Two algorithms were used to estimate latitude, the maximum slope method and the maximum logarithmic difference method. The broad-band, cosine-corrected light, excluding those deployments near the equinox when error is highest, produced an estimate of latitude of 38.30° for both methods and a latitudinal error of ±34.4 km for the former and ±27.2 km for the latter. The mean latitudinal error for non-cosine-collected, broad-band irradiance was ±190.9 km, using the slope algorithm and ±184.8 km using the difference algorithm. The blue band of irradiance, which attenuates least with increasing depth in clear, oceanic water, also produced a comparatively high-latitudinal error of ±163.8 km error for the former algorithm and ±170.4 km for the latter algorithm. Tag designers should consider using cosine-collectors over the irradiance sensors on their archival tags to increase the accuracy of position estimates.

Communicated by J.P. Grassle, New Brunswick.

H. A. Qayum
Cooperative Institute for Marine Resource Studies, Hatfield Marine Science Center, Oregon State University, 2030 S.E. Marine Science Drive, Newport, OR 97365, USA
e-mail: hisham.qayum@oregonstate.edu

A. P. Klimley (✉) · J. E. Richert
Department of Wildlife, Fish, and Conservation Biology, University of California, Davis, One Shields Avenue, Davis, CA 95616, USA
e-mail: apklimley@ucdavis.edu

J. E. Richert
e-mail: jerichert@ucdavis.edu

R. Newton
Tahoe Research and Development, 2230 Damon Road, Carson City, NV 89701, USA
e-mail: NewtonRon@netscape.net

Introduction

The development of electronic tags for long-distance tracking of pelagic fishes is of great interest to fisheries biologists and policymakers (for reviews of electronic

tagging and fisheries, see Hunter et al. 1986; Arnold and Dewar 2001; Gunn and Block 2001) because pelagic species such as sharks (e.g., Boustany et al. 2002; Bonfil et al. 2005) and tunas (e.g., Block et al. 2005) migrate ocean wide and must be managed across national boundaries. One device capable of long-distance tracking of fishes is the archival tag, which is a microprocessor-based recorder with sensors to measure behavioral properties such as heading, depth, and speed and environmental properties such as subsurface irradiance and water temperature. These measurements, or a processed subset of them, are stored in electronic memory aboard the tag. A daily geographic position, termed a ''geolocation,'' can be inferred for a tag holder from measurements of environmental properties such as submarine illumination (Hill 1994; Klimley et al. 1994; Welch and Evesen 1999; Hill and Braun 2001; Musyl et al. 2001; Welch and Eveson 2001), water temperature (Smith and Goodman 1986; Domeier et al. 2004; Teo et al. 2005), and bottom depth at different tidal states (Metcalfe and Arnold 1997).

Geolocating archival tags determine longitude using a method similar to that used by early mariners to navigate in the ocean. They found their longitude based on the difference between the ''apparent'' time, when they observed the sun was at its highest point in the sky at their current location, and the ''true'' time of noon, when the sun was at its highest point at a reference location (e.g., Greenwich, England). This time difference was recorded with an accurate clock, a chronometer. The archival tag similarly has a very accurate internal clock, which is initialized to Universal Time, yet is unable to find noon by the position of the disk of the sun because the fish tag is underwater and unable to distinguish celestial objects. Alternatively, the tag estimates the times of sunrise and sunset from rapid changes in the intensity of ''irradiance'' (energy in wavelengths near the visible region of the electromagnetic spectrum) at dawn and dusk, respectively (Hill 1994; Klimley et al. 1994; Ekstrom 2002, 2005). Apparent noon, midway between the rapid increase in light at sunrise and the rapid decrease in light at sunset, can be compared to true noon to determine longitude—each hour difference between apparent and true noon equals an offset of 15° from the prime meridian on the circumference of the earth. This is the basis of current longitude estimates, with corrections applied from the standard astronomical equations (Nautical Almanac Office 1997). An archival tag can also estimate latitude on the basis of irradiance measurements. Day length, or the time between sunrise and sunset (or conversely night length), varies with distance along a meridian on the earth's surface, and thus is an indicator of latitude except during the equinox, when the durations of daytime and nighttime are equal over the earth (Hill 1994; Klimley et al. 1994; Hill and Braun 2001). The length of the day (or night) at the established longitude at the known time of the year is then entered into a mathematical algorithm that solves for latitude. This algorithm is based on a series of astronomical equations (Nautical Almanac Office 1997) relating the rotation of the earth to its path around the sun. ''Threshhold'' methods relate a change in the intensity of irradiance to a solar angle (see Hill 1994; Welch and Evesen 1999; Hill and Braun 2001; Musyl et al. 2001; Welch and Eveson 2001); a ''template'' method, currently under development, fits an idealized curve to a series of irradiance intensities at dawn or dusk (Ekstrom 2002, 2005).

The purpose of our study was to compare the accuracy of estimates of latitude based on measurements of broad-band irradiance to estimates of latitude based on narrow-band measurements of irradiance. The former contained energy within the visible electromagnetic spectrum, a 400-nm band of wavelengths from 300 to 700 nm; the latter contained energy in 30-nm bands with their peak intensities separated by 50-nm intervals over the same broad range of wavelengths. The choice of a particular band of irradiance is critical for the estimation of a geolocation because irradiance of different wavelengths is absorbed at different rates in oceanic waters of varying clarity and this affects the rate of attenuation. Jerlov (1976) classified water types on the basis of their absorbance of various wavelengths with depth. Dissolved organic components, known as ''gelbstoff'' or ''marine snow,'' absorb irradiance energy strongly at the blue end of the spectrum. Blue irradiance (450 nm) penetrates deeper than green irradiance (550 nm) in the clearest oceanic waters, but green penetrates farther than blue irradiance in most oceanic and coastal waters. The designer of an archival tag for tracking the movements of fishes is presented with a dilemma. One can record blue irradiance, which transmits best in oceanic waters, or green irradiance, which transmits best in coastal waters. Alternatively, one can record broad-band irradiance that penetrates deeply in both types of water.

We used a highly sensitive, multi-spectral radiometer to measure broad-band and narrow-band irradiance at Horseshoe Cove, Central California, in water intermediate in its transmission properties between oceanic and coastal waters (Jerlov 1976). Two different algorithms were applied to these time series of irradiance measurements to identify the best bandwidth for estimating latitude. The objective of our study was to address concerns raised at a workshop (Metcalfe 2001)

about the need for archival tags to record the optimal wavelength(s) for determining accurate latitudes.

Methods

Irradiance measurement

To compare the effectiveness of broad and narrow band irradiance at estimating latitude, we followed the example of the software engineer, who for the sake of simplicity evaluates the ''benchmark'' speed that a newly created computer program takes to complete a given number of simple operations. Hence, we recorded irradiance at a single location (38.31°N; 123.08°W) in Horseshoe Cove, Bodega Bay and depth (10 m) for 1- and 2-day periods separated by two-week intervals from the summer solstice through the autumnal equinox (i.e., June 21–October 6, 1999). The accuracy of estimates of latitude were anticipated to vary over this period, being most accurate near the solstice, when day length varies most with latitude in the northern hemisphere, and least accurate near the equinox (September 23), when day length varies least with latitude.

Irradiance was measured in Horseshoe Cove because its water's transmission properties were intermediate between coastal and oceanic water (Jerlov 1976). We chose a depth of 10 m for two reasons. First, pelagic fishes usually swim at depths ≥10 m (e.g., sharks: Carey 1990; Klimley et al. 1994, 2002; billfishes: Holland et al. 1990b; Block et al. 1992; tunas: Holland et al. 1990a; Block et al. 1997). Second, we wanted the radiometer shallow enough to detect irradiance within the narrow bands even at night, when there is little subsurface irradiance aside from the moon and stars.

Underwater irradiance was measured with a multispectral radiometer designed and fabricated by one of the authors (RN). It possessed a highly light-sensitive, logarithmic amplifier, capable of detecting irradiance levels decreasing in intensity over ten logarithmic units (powers of 10), that enabled us to measure the minute levels of irradiance present for the seven narrow bands, which varied greatly in their underwater transmittance. This amplifier was continuously heated to maintain it at a constant temperature, and this required considerable power, which limited our sampling to 24–48 h per deployment. The intensity of irradiance was measured every 15 s for seven narrow bands of irradiance and two broad bands of light. The energy in the narrow bands peaked at 400, 450, 500, 550, 600, 650, and 700 nm, producing the following colors in the visible spectrum, violet, blue, blue–green, green, yellow, orange, and red. The energy in the broad-band was evenly distributed between 400 and 700 nm, and this white irradiance was either attenuated using neutral density filters or cosine-corrected using an optical diffuser. The holographic, cosine collector reduced the vertical transmission of irradiance and increased horizontal transmission of irradiance onto the surface of the photodiode and thus collected the more diffuse irradiance that exists at dawn and dusk. Most of the shorter wavelengths are scattered by dust in the lower atmosphere as they pass parallel to the earth's curvature (hence, the setting sun is red); these shorter wavelengths are scattered less in the upper atmosphere and give the sky a blue color during dawn and dusk (Ekstrom 2005). The design and operation of the radiometer are described in more detail in the Appendix.

The radiometer was deployed seven times in Horseshoe Cover. The first six deployments (days 7, 24, 38, 51, 64, and 93) occurred between the summer solstice, June 21, 1999 (day 0), and autumnal equinox, September 23, 1999 (day 94). The unit was deployed a seventh time on October 5 (day 106), 12 days after the autumnal equinox. The dates of the deployments are given along with their corresponding intervals relative to the vernal solstice in Table 1. The positional estimates thus would be expected to vary in accuracy from highest during the summer solstice, when the duration of day length varied most over the northern hemisphere, and least during the autumnal equinox, when the duration of day length varied least over the northern hemisphere. A storm precluded recovery of the radiometer after the seventh deployment, as it broke away from its mooring and was lost.

Setting and rising of the sun

It is important to define the solar events at dusk and dawn in order to fully understand how solar irradiance is used to estimate a geolocation. Sunset and sunrise are defined by the angle of the sun to the earth's horizon. The solar angle (α) is defined as the angle, measured in degrees, of the solar disk center either above (α is positive) or below (α is negative) the horizon (Fig. 1a). Geometrical sunset occurs when the ''upper limb'' or top of the sun's disk coincides with the horizon and its waist is 0.27° below the horizon (Fig. 1b). The observed sunset occurs later, when the waist of the sun is 0.82° below the horizon, because light bends (refracts) 0.55° around the earth's atmosphere, resulting in an apparent image of the sun after the sun has passed below the horizon (Nautical Almanac Office 1997). There is a period of time after sunset and before sunrise, twilight, when irradiance

Table 1 Dates, times, and durations of deployments of multi-spectral radiometer at a 10-m depth in Horseshoe Cove, Bodega Bay, California June 28–October 10, 1999

Number	*D*	Date (1999)		Time				
		Start	End	Start	End	Duration	Sunset	Noon
1	7	June 28	June 30	13:00:00	15:00:00	50:00:00	19:40	12:16
2	24	July 14	July 15	13:00:00	15:00:00	26:00:00	19:36	12:18
3	38	July 29	July 30	14:00:00	13:00:00	23:00:00	19:25	12:19
4	51	August 11	August 12	14:00:00	13:22:30	23:47:30	19:11	12:18
5	64	August 24	August 26	12:25:15	18:13:45	53:38:30	18:54	12:15
6	93	September 22	September 24	09:45:15	03:24:15	42:21:00	19:10	12:05
7	106	October 5	October 6	12:45:00	17:46:15	29:01:15	17:49	12:01

D (days) relative to vernal solstice on June 21, 1999. Autumnal equinox was on September 23, 1999 ($D = 94$). Times of sunset and noon (in PST) from US Naval Observatory

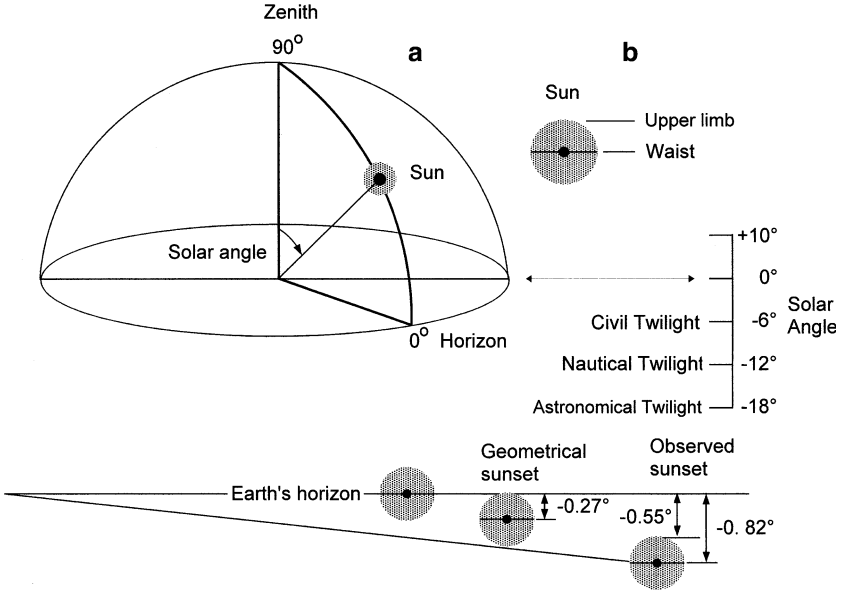

Fig. 1 Angle of sun is shown from apparent noon to twilight relative to the horizon of the earth (**a**) with transit of sun below horizon shown on expanded scale (**b**). Angular position of the sun is highest in the sky with a solar angle of 90° during apparent noon. Angle of the sun to horizon is –0.27° at geometrical sunset because its waist is below the horizon when its upper limb is tangent with the horizon. Observed sunset occurs when waist of the sun is 0.82° below the horizon, because light bends (refracts) 0.55° around the earth's atmosphere, resulting in an apparent image of the sun after the sun has actually passed below the horizon

originates only from the upper atmosphere, which receives direct sunlight and reflects part of it toward the surface of the earth (US Naval Observatory 2006). First is civil twilight, which terminates when the center of the solar disk is 6° below the horizon (or $\alpha = -6.0$). During this period, the illumination is adequate, under ideal weather conditions, to distinguish terrestrial objects from the dark background, see the horizon, and observe the brightest stars in the absence of the moon. Nautical twilight follows and continues until $\alpha = -12°$, and during this period the vague outlines of objects can be seen, but not the horizon. Astronomical twilight follows and expires at $\alpha = -18°$. During this period, the sun does not contribute directly to sky illumination, and the sky is practically imperceptible. The events are reversed in order during dawn.

Analysis of measurements

Measurements of irradiance intensity, stored as text files within the radiometer, were downloaded to a personal computer. Separate files for the measurements recorded at 15-s intervals were created for the broad and narrow bands. The measurements, which were originally in decimal format, were converted to logarithmic (base 10) format. Plots were made of a 2-h

period of measurements for each band during the first dusk on each deployment, an hour before to an hour after sunset, which was determined using software from the US Naval Observatory.

It was necessary to remove some of the short-term variation in the intensity of irradiance due to changes in cloud cover during dusk. There were fluctuations in the curves of the different bands of irradiance of 0.5 log unit during daytime and twilight and fluctuations of 1.0 log unit during the night. This photic noise is apparent in the saw-tooth nature curve of measurements of irradiance in the 550-nm bandwidth every 15 s for a 2-h period at dusk on August 24, 1999 (Fig. 2a). This photic noise was reduced substantially when a running average was calculated from five cells recorded over 1.25 min (Fig. 2b). Little additional reduction of noise was accomplished by increasing the number of values in the running average. Hence, five

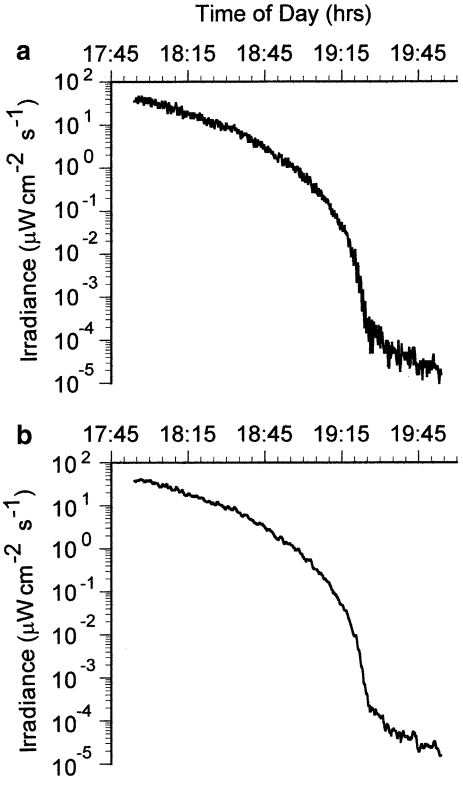

Fig. 2 Measurements of narrow band of irradiance with peak energy in 550 nm wavelength recorded at 15-s intervals over a period, 1 h before (17:45 h) sunset to 1-h after (19:45 h) at a depth of 10 m on a mooring in Bodega Bay on August 24, 1999. Un-averaged measurements (**a**) and running averages of five (**b**) measurements are plotted on logarithmic scale. Geolocation algorithms were then applied to a running average of five irradiance measurements to eliminate short-term fluctuations in irradiance intensity of ≤0.5 log units, yet to preserve irregularities in the irradiance curve due to true photic changes, which occur underwater as the sun passes below the horizon at sunset

irradiance measurements were averaged throughout the study.

We used two algorithms to estimate the latitudinal coordinate of the radiometer in Horseshoe Cove, California (38.31°N) from irradiance measurements, given its known longitude (123.08°W). The first algorithms involved finding the maximum slope of a curve fitted to irradiance measurements recorded at twilight. The second consisted of calculating the maximum difference between log-converted intensities subtracted from each other after an empirically determined separation interval. The first algorithm was developed by the senior author and the second resembles an algorithm used by Welch and Eveson (1999, 2001).

Maximum slope

This technique consisted of identifying the time corresponding to the maximum rate of change in irradiance intensity at dusk, relating this to the angle of the sun's disk center with respect to the horizon, and using this information to construct a linear fit to estimate the latitude of the radiometer for the known longitude. In particular, we plotted irradiance measurements at 15-s intervals over a period ranging from 1 h before to 1 h after sunset. We determined through inspection the time corresponding to maximum slope. A program developed by the first author, SolPeak, then fitted a 3rd order polynomial curve to a 30-min section centered about this initial estimate. The derivative of the corresponding polynomial equation identified the time corresponding to the maximum slope over the entire 2-h period. The program then found the angle of the sun at this time of day. The program identified the solar angle corresponding to the maximum slope, and then calculated the latitudes based on the solar angle along with the time corresponding to the maximum slope, and compared the result to the actual latitude. This constitutes the ''daily'' mode of geolocation.

SolPeak calculated the following statistics: the mean latitudinal error ($L_{\bar{e}}$), which is the mean of the absolute value of the deviations from the true latitude,

$$L_{\bar{e}} = \sum_{n=1}^{N} \frac{|L_{\text{est}} - L_{\text{ture}}|}{N}, \quad (1)$$

where L denotes latitude, as well as the correlation coefficient, slope, and y-intercept of a linear equation fitted to a plot of the solar angle relative to duration of the period (in days) after initial deployment of the radiometer, i.e., on June 28, 1999. We also calculated the angular mean and variance for the seven deploy-

ments, understanding that both solar angle and latitude were not decimal but angular variables. SolPeak also calculated, in the ''seasonal'' mode, the optimum solar angle and minimum latitudinal deviation from all the deployments. This calculation involved pairing the times corresponding to the maximum slope with 200 angular values at 0.1° intervals ranging from –10.0 to 9.9°, and selecting the angle that minimized the error between the calculated and true latitude of the radiometer.

Maximum logarithmic difference

We used a second method that amplified the change in intensity of irradiance associated with sunrise and sunset. The irradiance measurements were first converted to logarithmic format, after which the log of the intensity, log I_t, was subtracted from the log of intensity n minutes before, log I_{t-n}, to produce an amplified value of irradiance change, log I_a:

$$\log I_a = \log I_t - \log I_{t-n}. \quad (2)$$

Critical in the use of this algorithm was the choice of a time delay between log $I_{t=0}$ and log I_{t-n}, that maximized the change in intensity, but accomplished this over the shortest period of time to optimize resolution. Shown in Fig. 3c is the running average of logarithmic intensities of a wavelength of 550-nm irradiance during the 2-h period from 17:45 to 19:45 h at sunset on August 24–25, 1999. Above this curve (Fig. 1b) are four curves of the intensity gradients, calculated by subtracting from each intensity value the value recorded 1, 5, 10, and 15 min preceding it. A temporal separation of 5 min produced a peak that was both narrow and high (see arrows) relative to the other three intervals. The curve rose from a constant level of 0.0 log units at 18:05 h to a peak of 1.5 log units at 19:35 h before dropping to the former level at 19:45 h. The peak occurred when the sun was 7° below the horizon (Fig. 3a), long after the observed sunset at 18:54 h, and when the rapid attenuation of irradiance slowed after sunset (see arrow, Fig. 3c). The separation of 5 min produced the best ''marker'' because the upward ramping of intensity was more abrupt than for temporal separations of 10 and 15 min.

We performed the following steps to estimate latitude. We identified the time corresponding to maximum logarithmic change through visual inspection of a plot of irradiance intensities measured over a 2-h period, from 1 h before to 1 h after sunset. SolPeak then fitted a third order polynomial equation (chosen because of the single inflection to the curve) to a set of 25 irradiance intensities, each separated by 15-s, occurring before and after this initial estimate. The program then displayed the equation of the third order polynomial and a time corresponding to the maximum logarithmic change. The program later stored the corresponding solar angle and estimated latitude for multiple radiometer deployments. The same ''seasonal'' mode statistics were computed as with the maximum slope method.

Results

Diel cycle of irradiance

Intuitively, one would expect irradiance to change most rapidly as the equator of the sun passes below the earth's horizon. The amount of surface of the setting sun radiating solar energy at the horizon is greatest at this time, and hence the rate with which irradiance decreases at the horizon might be expected to be greatest. Yet irradiance at the observer (or radiometer) does not attenuate most rapidly at this time. This is apparent from a curve of the measurements of broad- and narrow-band irradiance from 15:00 h on August 24 to 09:00 h on August 25, 1999 (Fig. 4a) and a curve of the altitude of the sun relative to the horizon (Fig. 4c). The waist of the sun coincided with the horizon at 18:50 h; sunset occurred at 18:54 h when the upper limb of the sun was tangent with the horizon on August 24, 1999 (see Fig. 4c). Yet the cosine-collected, broad-band irradiance attenuated most rapidly well before 18:50 h (Fig. 4a), decreasing 270 μW m^2 s^{-1} over an hour-long period between 16:00 and 17:00 h with the elevation of sun's waist decreasing from a 30° to 25° angle relative to the horizon. Similarly, the broad-band irradiance that passed through a neutral density filter (see black curve) and irradiance of the seven narrow bandwidths decreased rapidly during the same period, but over a smaller range of intensities. This attenuation of irradiance also began well before the waist or upper limb of the sun passed below the horizon.

Another way of viewing the change in broad and narrow-band irradiance during sunset is to plot the measurements of irradiance on a logarithmic scale (Fig. 4b). The broad- and the narrow-band irradiance intensity was roughly constant from 15:00 to 16:00 h with fluctuations of 0.5 log unit that may have been due to the passage of clouds between the sun and earth. The intensity of cosine-corrected irradiance then decreased eight logarithmic units between 16:00 and 20:00 h. The irradiance began to attenuate most rapidly at 19:00 h, well after the waist of the sun passed

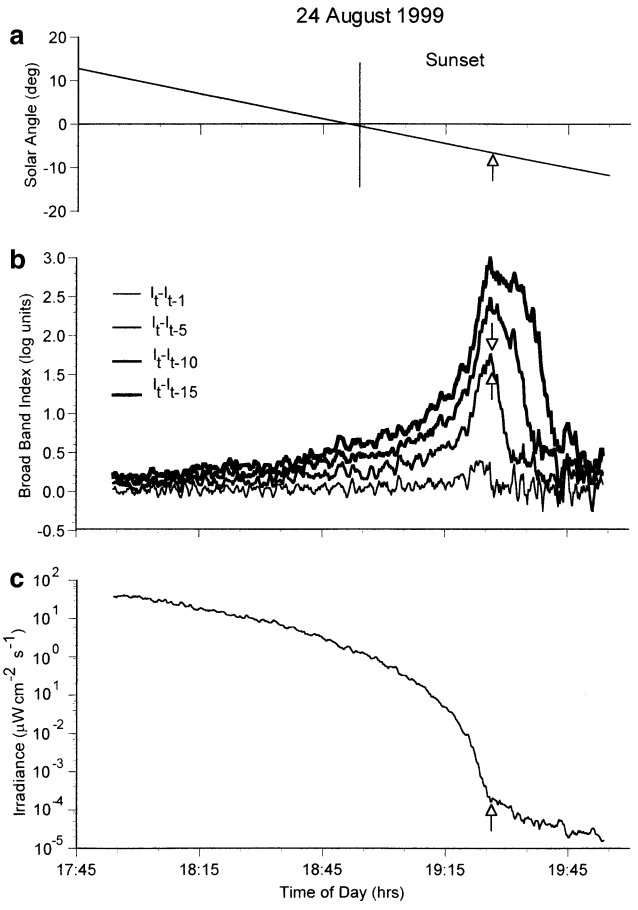

Fig. 3 Angle of sun relative to horizon is shown from 17:45 to 19:45 h on August 24, 1999 in Horseshoe Cove, Bodega Bay (**a**). Maximum logarithmic difference algorithm was applied to a running average of five measurements of the intensity of narrow band irradiance with a peak intensity of 550 nm. An interval over which values were subtracted from each other to produce a steep peak in logarithmic difference was determined, which was distinct from short-term fluctuations in the running average of measurements. Intensities were converted to log values and they were subtracted from each other after varying intervals of 1 (I_t–I_{t-1}), 5 (I_t–I_{t-5}), 10 (I_t–I_{t-10}), and 15 (I_t–I_{t-15}) min (**b**). Decrease in intensity of irradiance shown over same period (**c**). Peaks in four curves (**b**) coincided with discontinuities in slope of the curve of narrow band intensity over time (**c**). Subtraction of values at an interval of 5-min produced a peak (see *arrows* in **b** that was sufficiently distinct from the short-term, saw-tooth spikes in the curve to ascribe it to a unique solar angle (see *arrow* in **a**)

below the horizon at 18:50 h and sunset at 18:54 h. The nighttime level of broad-band irradiance then remained constant from 20:00 until the moon began to set at 01:30 h when the level decreased to a minimum at 04:30 h. Fluctuations in irradiance intensity of 0.5 log unit occurred while the moon was present, possibly due to clouds passing between the moon and the earth. The attenuation of narrow-band irradiance ranged from seven decades for green (550 nm) to four decades for violet (400 nm). The daytime intensities of the green irradiance averaged 4.0×10^2 μW cm^2 s^{-1}; the nighttime values averaged 4.0×10^{-5} μW cm^2 s^{-1}. The green and orange (650 nm) wavelengths decreased at dusk and increased at dawn more rapidly than the other five wavelengths. Note that the curves of logarithmically converted values of broad-band and narrow-band irradiance are more rounded and less steep than the curves on the linear plot (Fig. 4a). Furthermore, the levels of irradiance, expressed as logarithms to the base 10, decreased less rapidly before than after sunset while the same intensities, expressed as decimal values, decreased more rapidly before than after sunset. This is because the logarithmic conversion confers an equal value of one log unit to each power-of-ten reduction in the light intensity measured over the eight power-of-ten range of intensities. The conversion from linear into logarithmic values results in the same one logarithmic unit decrement in light intensity for the large change of 10–1 μW cm^{-2} s^{-1}, when the waist of the sun passed below the horizon at 18:30 h, as the small change at of 0.0001–0.00001 μW cm^{-2} s^{-1}at 19:20 h close to the end of nautical twilight. This conversion enhanced our ability to identify features in the irradiance curve for use in latitude determination.

Bandwidth comparisons with two algorithms

We determined the relative effectiveness of the two broad bands and the eight narrow bands at estimating the true latitude of the radiometer. Three indices were used, one that indicated the accuracy of the estimate, or closeness of the estimated latitude to the true latitude of the radiometer, another that denoted the precision of the estimate, or the similarity in values of repeated measurements, and an additional index that reflected both the accuracy and precision of the estimate. First, the mean latitude was calculated by summing the latitudes and dividing this total by the number of deployments. Second, the latitudinal variance was calculated subtracting the *mean estimated latitude* from each individually estimated latitude, taking its absolute value, squaring that value, adding all of the values, and finding the square root of the resulting sum. Third, the mean error was determined by subtracting the *true latitude* from each estimated latitude, taking the absolute value of each and adding them together, then dividing the resulting sum by the number of deployments.

Applying the maximum slope algorithm to the first five deployments, while excluding the last two near the equinox, to the cosine-collected, broad-band irradiance measurements resulted in a mean estimate of 38.30°N for the radiometer, which was situated at a latitude of

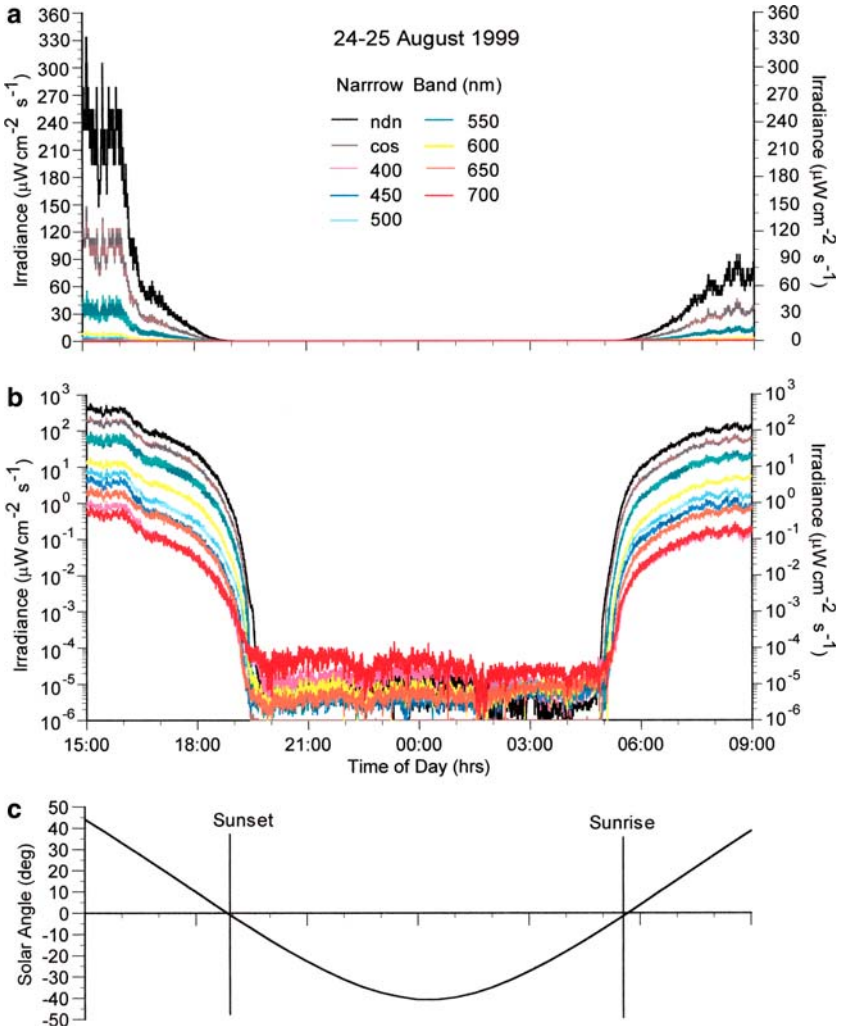

Fig. 4 Intensity of broad-band light and narrow-band irradiance plotted on linear scale at 15-s intervals from 15:00 to 09:00 h on August 24–25, 1999 in Horseshoe Cove, California (**a**). Broad-band light was recorded with either neutral density filter (*ndn*) or cosine-collecting filter (*cos*). Irradiance was also recorded within seven narrow bands with peak transmission at 400, 450, 500, 550, 600, 650, and 700 nm. Irradiance plotted on logarithmic scale at same intervals and over same period (**b**). Solar angle (altitude of sun) shown over same time period (**c**)

38.31°N (Table 2). The variation among the five estimated latitudes was the least of all bands of irradiance—the latitudinal variance was 0.73° and the mean latitudinal error was 0.62°. The maximum difference algorithm also produced a mean latitude of 38.30°N, a latitudinal variance of 0.62°, and a mean latitudinal error of 0.49° (Table 3). The ability of the cosine-collected irradiance to produce accurate daily estimates of latitude using both the maximum slope and difference algorithms is evident in plots of the estimated latitudes from six successive deployments of the radiometer (Fig. 5a, b). The estimates of the radiometer's position were very accurate between the summer solstice and the autumnal equinox, i.e., latitude estimates for days 7, 24, 38, 51, and 64 relative to the solstice. However, the positional estimate from both algorithms was less accurate near the equinox on day 94 with the estimated latitude of the radiometer being ≥42.00°N. In contrast, applying the same methods to broad-band measurements of irradiance by a photodiode not covered by a cosine collector resulted in a less accurate estimate of the mean position of the radiometer, 37.94° and 37.99°N, respectively (Tables 2, 3). But more significantly, the latitudinal variances and mean errors were much greater for the two algorithms, 3.52° and 3.44° for the maximum slope method and 3.46° and 3.33° for the peak difference method.

The best narrow bands for estimating the latitude of the radiometer using the slope method were the colors green (550 nm) and yellow (600 nm). The former's mean latitude of 38.30°N was slightly closer to the true latitude of the radiometer than the 38.28° of the latter. The latitudinal variance of 1.27° and mean latitudinal error of 1.07° for the green band were higher than the variance of 0.83° and error of 0.71° for the yellow band. The blue band, which attenuates least with increasing depth in clear, oceanic water, produced an accurate mean latitude of 38.30, but a very imprecise latitudinal variance of 3.37° and latitudinal error of 2.95°. All three narrow bands produced latitudinal estimates less

Table 2 Comparison of precision and accuracy of latitudinal determinations using greatest slope geopositioning algorithm in daily mode for multispectral radiometer during five deployments in Horseshoe Cove, California prior to the autumnal equinox

Type	Daily									Seasonal		
Band	A_{mn}	A_v	m	r	b	L_{mn}	L_v	$L_{\bar{e}}$	N_{dly}	A_{opt}	L_{rms}	N_{snl}
ndn	–6.04	2.52	–0.09	0.48	–3.39	37.94	3.52	3.44	5	–5.4	4.86	6
cos	–6.58	0.61	0.02	0.59	–7.29	38.30	0.73	0.62	5	–6.3	1.30	5
400	–5.47	3.00	–0.13	0.70	–1.64	38.32	3.33	3.21	5	–5.4	6.78	5
450	–3.73	1.38	0.03	0.16	–4.57	38.30	3.37	2.95	5	–4.0	3.66	5
500	–4.74	1.07	0.02	0.14	–5.35	38.33	2.35	2.17	5	–4.6	2.41	5
550	–5.97	0.67	0.01	0.16	–6.38	38.30	1.27	1.07	5	–5.9	1.39	5
600	–5.12	0.42	0.01	0.20	–5.42	38.28	0.83	0.71	5	–5.0	0.92	5
650	–2.99	0.75	–0.01	0.08	–2.67	38.27	1.55	1.29	5	–3.9	2.65	5
700	–2.29	1.65	–0.03	0.14	–1.36	38.20	4.25	3.54	5	–3.2	4.98	5

A_{mn} mean solar angle, A_v solar angular variance, m solar regression slope, r correlation coefficient, b regression y-intercept, L_{mn} mean latitude, L_v latitudinal variance, $L_{\bar{e}}$ mean latitudinal error, N_{dly} number of calculable days, *ndn* neutral-density filtered, *cos* cosine-corrected light

Table 3 Comparison of precision and accuracy of latitudinal determinations using peak difference geopositioning algorithm in daily mode for multispectral radiometer during five deployments in Horseshoe Cove, California prior to the autumnal equinox

Type	Daily									Seasonal		
Band	A_{mn}	A_v	m	R	b	L_{mn}	L_v	$L_{\bar{e}}$	N_{dly}	A_{opt}	L_{rms}	N_{snl}
ndn	–6.46	2.47	–0.085	0.480	–3.85	37.99	3.46	3.33	5	–7.2	4.65	6
cos	–7.15	0.53	0.021	0.491	–7.69	38.30	0.62	0.49	5	–7.0	1.07	5
400	–5.53	2.19	0.009	0.007	–5.79	37.61	5.36	4.77	5	–4.6	5.24	5
450	–4.11	1.50	0.034	0.205	–5.14	38.24	3.47	3.07	5	–4.1	3.67	5
500	–5.10	1.14	0.015	0.073	–5.57	38.27	2.55	2.35	5	–4.9	2.55	5
550	–6.38	0.69	0.007	0.043	–6.60	38.26	1.36	1.13	5	–6.2	1.38	5
600	–5.54	0.47	0.007	0.099	–5.76	38.28	1.00	0.81	5	–5.5	1.05	5
650	–3.60	0.55	0.008	0.095	–3.34	38.27	1.11	0.90	5	–3.9	1.35	5
700	–5.64	4.22	–0.192	0.839	0.24	38.26	3.45	3.29	5	–6.3	9.03	5

A_{mn} mean solar angle, A_v solar angular variance, m solar regression slope, r correlation coefficient, b regression y-intercept, L_{mn} mean latitude, L_v latitudinal variance, $L_{\bar{e}}$ mean latitudinal error, N_{dly} number of calculable days, *ndn* neutral-density filtered, *cos* cosine-corrected light

precise than those obtained using broad-band, cosine-collected irradiance. Using the maximum difference method, the yellow band (600 nm) was most accurate with an estimate of 38.28°N for the position of the radiometer with the lowest latitudinal variance of 1.00°N and mean latitudinal error of 0.81°N of any narrow band. The blue band with maximum underwater transmission provided an accurate estimate of the position of the radiometer with mean latitude of 38.24°, but the estimates were very imprecise—the latitudinal variance was 3.47° and the latitudinal error of 3.07°.

The superiority of the cosine-collected to non-cosine-collected, broad-band irradiance and to the narrow-band irradiance was also evident when geolocations were estimated based on measurements taken on day 93, 1 day before the autumnal equinox, and day 106, 12 days after the equinox. This is evident in a box plot, displaying the statistical data for all bands (Fig. 6). Note the solid horizontal line, indicating the median, was very close to the horizontal dotted line, denoting the latitude of the radiometer, and the open boxes, showing the range between the 25th and 75th percentages (an indicator of variability), were smallest for cosine-collected light using both the slope (Fig. 6a) and difference algorithms (Fig. 6b). Note the greater distance between the solid line, indicating the median estimated latitude, and dotted line, denoting true latitude, for the broad-band irradiance not recorded with the cosine collector, using both geolocation methods; moreover, the boxes indicating variability were far larger than those for the measurements of cosine-collected irradiance. The narrow band with median latitudinal estimates nearest to the true latitude of the

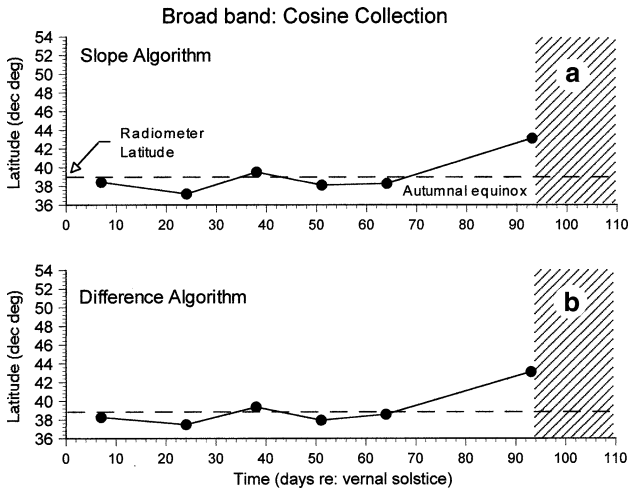

Fig. 5 Estimates of latitudes of radiometer (38.31°N) in Horseshoe Cove determined by applying the maximum slope (**a**) and maximum logarithmic difference (**b**) algorithms to curves of cosine-corrected light plotted as function of days following the vernal solstice on June 21, 1999, when variation in day length was greatest in northern hemisphere (cross-hatching denotes period following equinox)

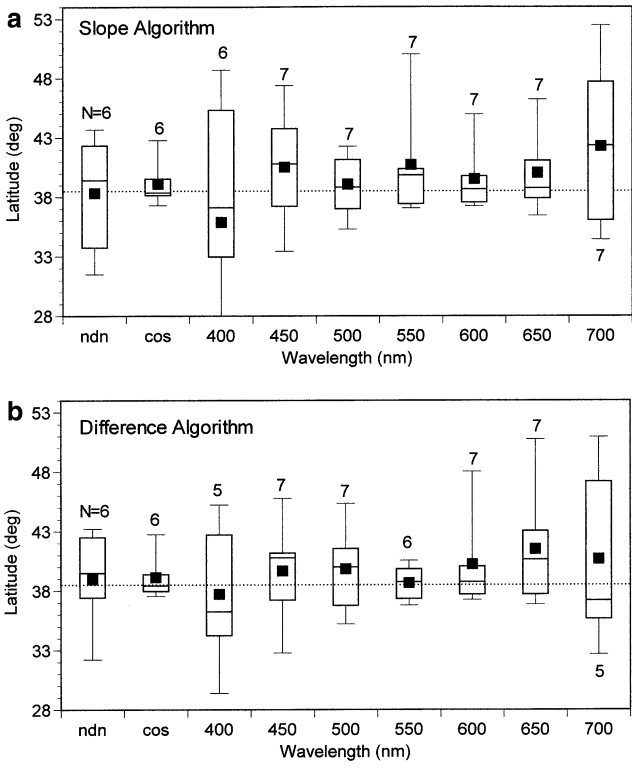

Fig. 6 Whisker plots of estimates of latitude of radiometer (38.38°N) in Horseshoe Cove for two broad bands of light [neutral density filtered (*ndn*) and cosine-collected (*cos*)] and seven narrow bands of irradiance (400, 450, 500, 550, 600, 650, and 700 nm) using maximum slope (**a**) and maximum logarithmic difference algorithms (**b**). On bars, lowest horizontal line corresponds to 10th, bottom of box to 25th, middle horizontal line 50th (median), top of box to 75th, and highest horizontal line, 90th percentile (ndn = neutral density, cos = cosine-corrected irradiance, stippled line = latitude of radiometer). Estimates were most accurate and precise for cosine-corrected light and narrow-band irradiance of 550 nm, indicated by proximity of *middle lines* (median latitude) to *stippled line* (radiometer latitude) and size of the boxes delineating the 25th–75th percentiles

radiometer was 600 nm for both methods, but its variation was far greater than that of the cosine-corrected irradiance.

It was thus not unexpected that cosine-corrected light produced a minimum latitudinal standard deviation of 1.30° from the position of the radiometer using the slope algorithm when a single optimal solar angle of –6.3° was used to estimate geolocation from irradiance measurements collected on days 7, 24, 38, 51, and 64 between the solar solstice and autumnal equinox (Table 2). The cosine corrected light produced a minimum latitudinal standard deviation of 1.07° for an optimal solar angle of –7.0° using the difference algorithm (Table 3). The minimum latitudinal error for the broad-band irradiance without a cosine collector was 4.86° for the slope method and 4.65° for the maximum difference method. Yellow irradiance of 600 nm provided slightly lower standard deviations of 0.92° and 1.05°, respectively. Green irradiance of 550 nm had slightly higher errors of 1.39° and 1.38° for the two algorithms; blue irradiance, which transmits with least attenuation in the open ocean, had much higher standard deviations of 3.66° and 3.67° for the two algorithms.

Discussion

A particular region of the electromagnetic spectrum must be selected from which to measure the intensity of irradiance periodically during the day to estimate a longitude and latitude. Does one select a broad region of the electromagnetic spectrum or a narrow region? Which bands decline in intensity rapidly as the sun descends below the horizon, or conversely, increase rapidly as the sun ascends above the horizon? What wavelengths in the electromagnetic spectrum penetrate deepest in the clearest oceanic waters? What wavelengths penetrate deepest in more turbid coastal waters? Current archival tags measure both broad- and narrow-band irradiance, either non-cosine-collected, broad-band irradiance at 400–700 nm (Roger Hill, Wildlife Computers, personal communication) or narrow-band irradiance centered at 450 nm (Phillip Ek-

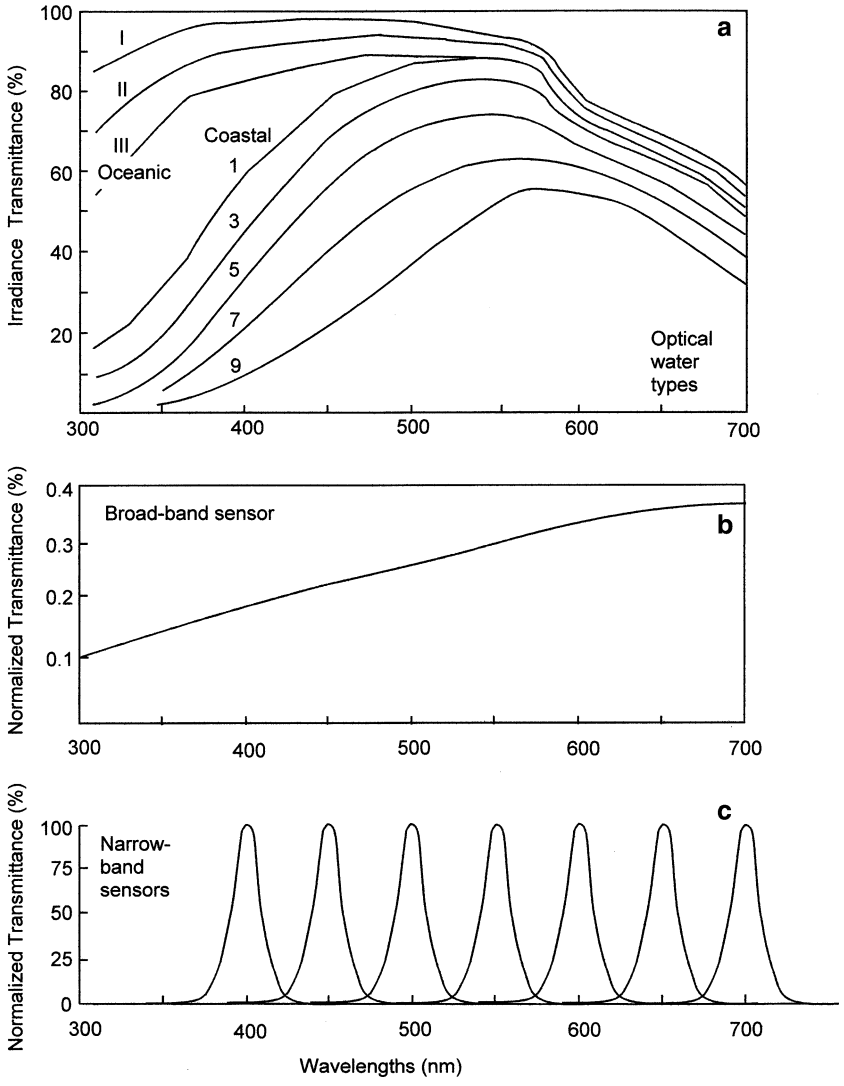

Fig. 7 Curves of transmittance relative to wavelength of light in oceanic waters, types I–III, and coastal waters, types I–IX (**a**), compared to normalized transmittance of two broad-band sensors (**b**) and seven narrow-band sensors (**c**)

strom, Northwest Technologies, personal communication).

To answer these questions, one must have some understanding of the behavior of light underwater. The intensity of cosine-corrected, broad-band irradiance changes by eight powers of ten at dusk and dawn and the intensity of narrow-band irradiance from seven to five powers of ten, depending upon whether it is green or red irradiance, respectively. Irradiance began to attenuate first at a solar angle of 30° relative to the horizon on both the linear and logarithmic curves, and this was due to the increasing amount of atmospheric absorption and reflection of light with the increasing angle of incidence. Sunset and sunrise appeared low on the shoulders of the linear curves; high on the shoulders of the logarithmic curves. This apparent discrepancy is due to the two different methods of expressing the attenuation of light at dusk and dawn. The linear plot displays the large initial decrease in the high-daytime intensities as the sun descends at dusk. The decrease in light intensity as the sun passes below the horizon is dwarfed by the earlier attenuation in the linear plot. The logarithmic plot gives equal weight to every power of ten decrease in irradiance intensity. Hence, the curves of broad-band irradiance apparently descend more slowly at dusk, and sunset is high on the curve.

Munz and McFarland (1973) recorded a decrease of seven powers of ten as above on August 23, 1970 in clear water during astronomical dusk over a coral reef at Eniwetak Atoll (11.5°N) of the Marshall Islands. Less light reaches the surface of the ocean as the sun moves lower in the sky and closer to the horizon before the sunsets, and more light energy is absorbed by passing through more of the earth's atmosphere. There is a familiar reddening of the western horizon due to a

rapid attenuation of the green, yellow, and orange light (550–650 nm) with the greatest reduction in energy at 60 min after sunset, when there are only 33% as many photons at these wavelengths compared to the narrow band of 450 nm (Munz and McFarland 1973). This results in a bimodal spectrum, which peaks at blue and red. The yellow–orange decline during twilight results specifically from its absorption by ozone as light passes through more of the atmosphere, and is called the Chappuis effect (Rozenberg 1966). Furthermore, more light is reflected off the surface of the ocean as the angle of incidence increases. We found that energy in the wavelengths of 650 (orange) and 700 (red) decreased to their nighttime levels before all other wavelengths except 400 nm (ultraviolet), but this was not so for a wavelength of 600 nm (yellow) as predicted by the Chappuis effect.

Jerlov (1976) classified water types on the basis of their absorbance of various wavelengths with depth. Dissolved organic components, known as ''gelbstoff'' or ''marine snow,'' absorb irradiance energy strongly at the blue end of the spectrum. Blue irradiance (450 nm) attenuates less with increasing depth than green irradiance (550 nm) in the clearest oceanic waters; green attenuates less than blue irradiance in most oceanic and coastal waters. Based on the difference in relative transmission of irradiance of varying wavelengths, Jerlov (1968) defined three types of oceanic water (types I–III) and nine types of coastal water (types I–IX) (Fig. 7a). In type I water, energy of the blue wavelength (450 nm) penetrates the ocean deeper than the energy in the green wavelength (550 nm)—this water type occurs in the tropics offshore of coasts in the absence of upwelling (see transmittance of narrow band filters in Fig. 7c). In type II water, blue and green irradiance attenuate equally with depth—this type of water is found at subtropical (20–30°) and temperate latitudes (30–60°). In type III water, green irradiance penetrates the ocean farther than blue—this water type is present offshore of tropical coasts during upwelling (e.g., western equatorial coasts of Africa and South America) and at polar latitudes (>60°). The transmission of green far exceeds that of blue irradiance in coastal types I–IX. The water close to shore in Central California, where we recorded measurements of irradiance and determined the accuracy and precision of geoposition estimates, is intermediate in its transmission properties between type 1 coastal and type II oceanic waters (see Fig. 72, Jerlov 1976).

Our radiometer recorded irradiance energy in two broad bands as well as eight narrow bands. The light recorded in the two broad bands were inclusive of the entire region of the visible electromagnetic spectrum penetrating the oceanic and coastal waters, yet the neutral density filtered sensor detected mainly down-welling light whereas the cosine-collecting sensor detected side and upwelling light as well. The 400–450 nm filters recorded irradiance that transmits best in clear, oligotrophic waters. The 500–550 nm filters recorded irradiance in turbid, eutrophic waters. One solution is to use a filter to match the sensor's spectral sensitivity to the optimum transmission in the waters, through which tagged fish are expected to migrate. The photodiode on tags on billfish, tunas, and some sharks, which live and migrate in clear tropical waters, would have a filter in the 400–450 nm range, whereas tags on coastal species and those in temperate and polar regions with turbid waters such as rockfish, groupers, salmons, and sturgeon would have a filter in the 500–550 nm range. The alternative solution is to choose a cosine-correcting filter, which will collect all irradiance from 400 to 700 nm. This option also maximizes the irradiance recorded at twilight, when much of the irradiance is reflected in the form of side and down-welling light.

The level of the cosine-collected irradiance was always higher than unfiltered light and the eight narrow bands later during dusk. This is because the cosine collector is more sensitive to subsurface, reflected light impinging at an angle of 90° (horizontal) and less sensitive to light accepted at an angle of 0° (vertical). As the sun passed lower on the horizon, a greater percentage of the light impinging directly on the sea surface is reflected, and there is a smaller proportion of down-welling light to indirect up- and side-welling light in the water column (Jerlov 1976; Drew 1984). The broad-band sensor with a cosine collector is more sensitive to this indirect light, and will thus record greater levels of irradiance at dusk than a light or narrow-band sensor.

We found that, using the maximum slope algorithm, the cosine-collected, broad-band irradiance produced the lowest mean latitudinal error of ±34.4 km, for the five deployments of the radiometer. The mean latitudinal error for non-cosine-collected, broad-band irradiance was ±190.9 km. In a study at 54°N., Welch and Eveson (1999) estimated latitude based measurements of broad-band irradiance of 400–700 nm made by four Wildlife Computers archival tags that were attached to the offshore mooring in type II water at a 10-m depth from March 9 (near equinox) to June 12, 1997 (near solstice). Day length was defined as the period between the times of maximal change of broad-band, irradiance intensity at dawn and dusk. They identified a maximum slope, selected a symmetrical range of values to either side, fitted a polynomial equation to the values, and

differentiated the fitted equation to estimate the times of dawn or dusk. They concluded that latitude was estimated by the tags with an average error of ±65.0 km.

Our best performing narrow band (yellow, 600 nm) estimated latitude with an error of ±39.4 km, much more accurate than the ±163.8 km error for blue irradiance, which penetrates farthest in oceanic water. In a study at 24°N., Musyl et al. (2001) found mean latitudinal error of ±84.8 km in type I water using the same technique for three Northwest Marine Technology archival tags with a narrow-band filter recording blue irradiance of 450 nm. The tags were attached to an offshore mooring at a 20-m depth for nearly a year from August 29, 1998 to August 16, 1999.

Hill (1994) first estimated the latitude of an archival tag by defining day length as the period between two points on a light curve based on a percentage of the height of a logarithmic light curve. He defined sunset with a solar angle of 0.83° relative to the horizon to be 50% of the light curve; dusk with a solar angle of –6.00° to be 5% of the light curve. Welch and Eveson (1999) also estimated latitude as a percentage of the curve of irradiance measurements made at 54°N. Daytime and nighttime levels of irradiance were estimated by averaging the light readings within a 2.5-h span on either side of local noon and midnight. They applied a two-stage, curve-fitting process to estimate the time at which the reference light level was reached. They recorded an error of ±66.8 km in estimates of the latitude of four Wildlife Computer archival tags, which were sensitive to broad-band irradiance. In a more recent study at 48.8°N (Welch and Eveson 2001), they found mean latitudinal error of ±44.0 km in estimating the position of six Wildlife Computer archival tags, also sensitive to broad-band irradiance, at a 15-m depth on a mooring in the eastern North Pacific Ocean. We were unable to evaluate this technique rigorously because of the low numbers of irradiance curves to which the algorithm could be applied and produced a solution (unpublished data). Musyl et al. (2001) determined mean errors for a Northwest Marine Technology archival tag, which recorded narrow-band irradiance peaking at 450 nm, using the percentage method. The first method produced a mean error of ±116.3 km and the second, more dynamic method produced a mean error of ±78.1 km in estimating the latitude of the tag deployed at a depth of 20 m on the oceanographic mooring. Manually removing outliers in the data improved the precision of the latitudinal estimates to ±96.4 and ±64.3 km, respectively.

We found greater accuracy and precision in latitudinal estimates using cosine-corrected irradiance at the study site than either the non-cosine-collected broad-band or narrow-band irradiance when utilizing both the maximum slope and difference algorithms. The advantage of the cosine-collector is that it absorbs irradiance equally from angles of incidence of 0° (vertical) to 90° (horizontal). Hence, more irradiance was absorbed by the cosine-corrected, broad-band sensor as the sun set and the angle of incidence was higher than non-cosine-collected, broad-band sensor or the narrow-band irradiance sensors. The performance of narrow-band sensors depends upon the type of water. As dissolved and particulate matter increases in sea water, there is a shift in maximum transmittance from the blue–green to the green–orange region of the spectrum. Thus, one should choose a sensor that records irradiance of a particular wavelength that has maximum transmittance in the region of the ocean where fish being tracked. A broad-band sensor sensitive to irradiance of 400–700 nm has the advantage of detecting irradiance of multiple wavelengths in multiple types of water and furthermore collects more energy at greater depths than a narrow-band sensor. Tag designers should consider using cosine-collectors over their broad-band irradiance sensors to increase the accuracy of position estimates.

Acknowledgments This work was supported by a grant to APK by the National Undersea Research Program (NOAA) and the Marine Technology Program of the National Science Foundation. Tagging of Pacific Pelagics (TOPP) with direction from B.Block, kindly paid for the curves of spectral intensity to be reproduced in their corresponding colors. We appreciated the assistance of S. Beavers, T. Curtis, and S. Jorgensen during various phases of the study.We want to thank David Welch, who openly reviewed an earlier version, and four anonymous reviewers, who vastly improved this article. H. Fastenau, T. McCrumman, and K. Menard deployed the radiometer underwater at two-week intervals during the study.

Appendix

Design and operation of multi-spectral radiometer

We measured the intensities of underwater irradiance with a multi-spectral radiometer designed and fabricated by one of the authors (RN). The device recorded the intensity of irradiance in seven narrow bands of irradiance and two broad bands of light. Peak absorption in the narrow bands was in the following wavelengths, 350, 400, 450, 500, 550, 600, 650, and 700 nm, corresponding to colors in the visible spectrum of ultraviolet, blue, blue green, green, yellow, orange, and red. The energy in the broad bands of light was distributed equally over the seven wavelengths in the visible spectrum, and was either attenuated using

neutral density filters (*ndn*) or cosine-corrected (*cos*) using an optical diffuser. ''Light'' is defined as the broad band of wavelengths perceptible by to the human eye.

The radiometer was capable of recording irradiance over the range of 10 log units that occur between local noon and midnight in the absence of moonlight. A heated amplifier (Dawn Electronics, DN120, Charlottown, PE, Canada) converted the linear output of a photocell (Hamamatsu, S1227-1010BQ) resulting from the gradient in the flux of light impinging on the cell into an output, unaffected by the daily temperature fluctuations in the marine environment. The radiometer had a circular disk with nine holes for optical filters and one solid region in a circular configuration that rapidly rotated so that each filter would be above a single photodiode and broad or narrow-band irradiance measurement recorded every 15 s. Seven narrow-band filters (Andover Corp., Salem, NH, USA 110FA40-12.5) were inset in the holes. The disk rotated 360° over ten evenly spaced photodiodes to record ten measurements, one of which was the ''dark'' current produced in the absence of light. The passage of other wavelengths through the narrow band filters decreased to 50% of the peak wavelength within 15 nm on either side of each transmission peak. A neutral density filter (Andover Corp, 030FN52-1125), reducing transmission by 50%, was placed in the eighth hole; a holographic light diffuser (Physical Optics Corp., LSD, Torrance, CA, USA) in the ninth hole evenly weighted incoming light over an 180° angle. These diffusers enable the transmission of 80–90% of the light impinging on the surface of a sensor over angles ≤90°. The output from the logarithmic amplifier was converted to a digital signal by a 256 A/D converter with 25 bits available for each decade of amplification. The radiometer contained a microprocessor (Microchip Technology Inc., PIC 16C71, Chandler, AZ, USA), which operated on RISC instruction code in EPROM, and stored the irradiance measurements in SRAM. The amount of memory in the unit permitted operation for 27 h, and it was necessary to charge the unit, before redeploying it again. We programmed the unit and downloaded data using a BASIC program.

The output from the radiometers in response to different levels of irradiance was expressed in milliamps recorded per light levels. The output of the photodiode increased linearly with the input of radiant flux in watts in a 1:1 ratio (see ''linearity'' graph for S1227-1010BQ, Hamamatsu Product Brochure). Hence, we are relatively confident that the change in output of the radiometers was proportional to the change of underwater irradiance. We measured the irradiance change in absolute physical units within the narrow band centered at 550 nm recorded by the multi-spectral radiometer. Irradiance of this wavelength is 120 μW cm^{-2} s^{-1} at sea level (Ryer 1988). The output (in current) of the 550-nm channel of the radiometer at a depth of 10 m was 0.27 of its output at the surface at the same time during midday. This provided a reference for the peak daytime underwater irradiance of 550 nm of 32.4 μW cm^2 s^{-1}. This value was decreased linearly in a 1:1 ratio relative to the output of the 550-nm channel of the radiometer to describe the dynamic range of irradiance intensity between night and day under water.

References

Arnold G, Dewar H (2001) Electronic tags in marine fisheries research: a 30-year perspective. In: Sibert JR, Nielsen JL (eds) Electronic tagging and tracking in marine fisheries. Kluwer Academic Publishers, Dordrecht, pp 7–64

Batschelet E (1981) Circular statistics in biology. Academic Press, London

Block BA, Booth DT, Carey FG (1992) Depth and temperature of the blue marlin, *Makaira nigricans*, observed by acoustic telemetry. Mar Biol 114:175–183

Block BA, Keen JE, Castillo B, Dewar H, Freund EV, Marcinek DJ, Brill RW, Farwell C (1997) Environmental preferences of yellowfin tuna (*Thunnus albacares*) at the northern extent of its range. Mar Biol 130:119–132

Block BA, Teo SLH, Wall A, Boustany A, Stokesbury MJW, Farwell CJ, Weng KC, Dewar H, Williams TD (2005) Electronic tagging and population structure of Atlantic bluefin tuna. Nature 434:1121–1127

Bonfil R, Me M, Scholl MC, Johnson R, O'Brien S, Oosthuizen H, Swanson S, Kotze D, Paterson M (2005) Transoceanic migration, spatial dynamics, and population linkages of white sharks. Science 310:100–103

Boustany AM, Davis SF, Pyle P, Anderson SD, Le Boeuf BJ, Block BA (2002) Expanded niche for white sharks. Nature 415:35–36

Carey FG, Scharold JV (1990) Movements of blue sharks (*Prionace glauca*) in depth and course. Mar Biol 106:329–342

Domeier ML, Kiefer D, Nasby-Lucas N, Wagschal A, O'Brien F (2004) Tracking Pacific bluefin tuna (*Thunnus thynnus orientalis*) in the northeastern Pacific with an automated algorithm that estimates latitude by matching sea-surface temperature data from satellite with temperature data from tags on fish. Fish Bull 103:292–306

Drew EA (1984) Light. In: Earll R, Erwin DG (eds) Sublittoral ecology. Clarenden Press, Oxford, pp 10–57

Eckstrom P (2002) Blue twilight in a simple atmosphere. Society of Photo-Optical Instrumentation Engineers (SPIE), Proceedings of SPIE, 4815, Paper 14

Eckstrom P (2005) An advance in geolocation by light. Lotek Wireless, St.John's, Canada

Gunn J, Block BA (2001) Advances in acoustic, archival, and satellite tagging of tunas. In: Block BA, Stevens ED (eds)

Tuna physiology, ecology, and evolution. Academic Press, San Diego, CA, pp 167–224
Hill RD (1994) Theory of geolocation by light levels. In: Le Boeuf BJ, Laws RM (eds) Elephant seals: population ecology, behavior, and physiology. University of California Press, Berkeley, pp 227–236
Hill RD, Braun MJ (2001) Geolocation by light level—the next step: latitude. In: Sibert JR, Nielsen JL (eds) Electronic tagging and tracking in marine fisheries. Kluwer Academic Publishers, Dordrecht, pp 315–330
Holland KN, Brill RW, Chang R (1990a) Horizontal and vertical movements of yellowfin and bigeye tuna associated with fish aggregating devices. Fish Bull 88:493–507
Holland KN, Brill RW, Chang RKC (1990b) Horizontal and vertical movements of Pacific blue marlin captured and released using sportfishing gear. Fish Bull 88:397–402
Hunter JR, Argue AW, Bayliff WH, Dizon AE, Fonteneau A, Goodman D, Seckel GS (1986) The dynamics of tuna movements: an evaluation of past and future research. FAO Fish Tech Pap 277:1–78
Jerlov NG (1968) Optical oceanography. Elsevier Oceanography series 5, Elsevier Scientific Publishing Company, Amsterdam
Jerlov NG (1976) Marine optics. Elsevier Ocean series 14, Elsevier Scientific Publishing Company, Amsterdam
Klimley AP, Prince ED, Brill RW, Holland K (1994) Archival tags 1994: present and future. NOAA Tech Mem NMFS-SEFC-357
Klimley AP, Beavers SC, Curtis TH, Jorgensen SJ (2002) Movements and swimming behavior of three species of sharks in La Jolla Canyon, California. Environ Biol Fish 63:117–135
Metcalfe JD (2001) Summary report of the workshop on daylight measurements for geolocation in animal telemetry. In: Sibert JR, Nielsen JL (eds) Electronic tagging and tracking in marine fisheries. Kluwer Academic Publishers, Dordrecht, pp 331–342
Metcalfe JD, Arnold GP (1997) Tracking fish with electronic tags. Nature 387:665–666
Munz FW, McFarland WN (1973) The significance of spectral position in the rhodopsins of tropical marine fishes. Vision Res 13:1829–1874
Musyl MK, Brill RW, Curran DS, Gunn JS, Hartog JR, Hill RD, Welch DW, Eveson JP, Boggs CH, Brainard RE (2001) Ability of archival tags to provide estimates of geographical position based on light intensity. In: Sibert JR, Nielsen JL (eds) Electronic tagging and tracking in marine fisheries. Kluwer Academic Publishers, Dordrecht, pp 343–367
Nautical Almanac Office (1997) The astronomical almanac. Supplementary data from the Time Service Department of United States Naval Observatory. US Printing Office, Washington DC
Rozenberg GV (1966) Twilight—a study in atmospheric optics. Plenum Press, New York
Ryer A (1998) Light measurement handbook. International Light Inc., San Diego
Smith P, Goodman D (1986) Determining fish movements from an archival tag: precision of geographical positions made from a time series of swimming temperature and depth. NOAA Tech Mem, Southwest Fish Cent 60:1–13
Teo SLH, Boustany A, Blackwell S, Walli A, Weng KC, Block BA (2004) Validation of geolocation estimates based on light level and sea surface temperature from electronic tags. Mar Ecol Progr Ser 283:81–98
US Naval Observatory (2006) Rise, set, and twilight definitions. http://aa.usno.navy.mil/faq /docs/RST_defs.html
Welch DW, Eveson JP (1999) An assessment of light-based geoposition estimates from archival tags. Can J Fish Aquat Sci 56:1317–1327
Welch DW, Eveson JP (2001) Recent progress in estimated geoposition using daylight. In: Sibert JR, Nielsen JL (eds) Electronic tagging and tracking in marine fisheries. Kluwer Academic Publishers, Dordrecht, pp 369–383